



ethane ( $C_2H_6$ ), well-known gaseous products and tracers of biomass burning, are utilized for this communication.

### 3. Methodology

[9] The AHSRL acquires *b* and *d* profiles at 2.5 second temporal resolution and at an altitude resolution of 7.5 m across a recorded range of 30 km. Since the derived optical profiles acquired at the nominal temporal resolution can be noisy in the presence of the weak optical signals typical of the Arctic environment, we further averaged the optical profiles to achieve a sampling resolution that better matched the three-minute CIMEL sampling resolution. AHSRL *b* profiles yield extinction coefficient profiles which can be integrated to obtain an estimate of total optical depth at 532 nm. These profiles are obtained by assuming typical values for the aerosol extinction to backscatter ratio or by exploiting the HSRL molecular/aerosol discrimination capability to perform a direct computation using a spatial derivative approach. The *d* profiles permit one to distinguish between aerosols with low *d* values (sub-micron smoke or pollution aerosols) and irregularly shaped supermicron particles such as ice crystals and irregularly shaped coarse mode aerosols (dust being a relevant example).

[10] The PEARL AODs were acquired in a high frequency (3-minute) temporal mode across eight spectral channels (nominally 340, 380, 440, 500, 675, 870, 1020, and 1640 nm). A six-channel subset (380, 440, 500, 675, 870, and 1020 nm) was employed in retrieving the total, fine mode and coarse mode optical depths at 500 nm (AOD or  $t_a$ ,  $t_f$  and  $t_c$  where  $t_a = t_f + t_c$ ) using the spectral deconvolution algorithm (SDA) of O'Neill et al. [2003]. We employed level 1.0 (non-cloud-screened) AERONET data in order to better understand the detailed variations which could be seen in both the AHSRL and optical depth data.  $t_f$  retrievals allow one to delineate sub-micron events such as sulphate based pollution and smoke from coarse mode events such as dust incursions and thin cloud [O'Neill et al., 2008, 2003]. The difficulty of employing a (spectral) curvature-based retrieval method in clear atmospheres such as those of the Arctic is that the error varies roughly as the inverse of the AOD [O'Neill et al., 2008, 2003]. The AHSRL *b* retrievals are themselves also sensitive to small signals. We accordingly tried to maintain a degree of healthy scepticism when analyzing the combination of AHSRL and sunphotometry retrievals.

[11] Bruker FTS spectra were collected during clear sky conditions, and generally consist of four co-added spectra at a resolution of  $0.0035\text{ cm}^{-1}$  (where resolution is  $0.9/\text{maximum optical path difference}$ ). Partial column amounts of CO and  $C_2H_6$  between 0.61 km (the elevation of PEARL) and 10 km (approximate tropopause height) have been determined from profiles retrieved using the SFIT2 algorithm [e.g., Pougatchev et al., 1995; Rinsland et al., 1998]. Synthetic spectra in one or more narrow wavenumber regions (in this case, three regions between 2057 and  $2159\text{ cm}^{-1}$  for CO, and one region between 2976.5 and  $2977.2\text{ cm}^{-1}$  for  $C_2H_6$ ) are fitted to the measured solar absorption spectra using the optimal estimation technique of Rodgers [2000]. The degrees of freedom of signal for these partial column measurements [Rodgers, 2000] are approximately 2.1 and 1.1 for CO and  $C_2H_6$  respectively, with

random error typically 2–4.5% for CO and 5–8% for  $C_2H_6$  [Rinsland et al., 1998; Zhao et al., 2002].

### 4. Results

[12] Figure 1 shows two sample smoke events which were traced back to forest fires in disparate regions of Russia (north of the city of Khabarovsk, near the Chinese border and north of the Kamchatka Peninsula). The broken purple lines delineate rough optical limits for these events.

[13] Figure 2 is a typical example of the type of evidence put together to support our contentions concerning the smoke origins of optical disturbances such as those seen in Figure 1. The graphical ensemble of Figure 2 was designed to be as self evident as possible with purple and orange colour codes being employed to approximately outline equivalent areas on the different images or maps. The MODIS visible & short-wave infrared (SWIR) images, apart from identifying hot spots, lend qualitative support to the affirmation that the hazy plumes seen in the visible-band imagery is sub-micron smoke (plume backscatter would be weak in the SWIR band as a consequence of the rapid spectral decrease of optical depth for small-particle smoke).

[14] The red  $t_f$  curve of Figure 1a shows qualitative correlation with the *b* plume (2nd row of graphs) at around 9 km altitude while the corresponding *d* values in the third row of graphs appear to be systematically small amidst a clutter of noise. The optical thickness of this plume was estimated to be 0.025 using extinction coefficients derived from spatial derivatives of the AHSRL *b* profiles; this is in approximate agreement with the  $t_f$  variation which was

0.020. Extreme excursions in  $t_c$  (blue curve) correspond to strong *b* signals on July 23 and 24 which, in turn, correspond to elevated (reddish) *d* values; the strong  $t_c$  variation and the high *d* values indicate that these events are most likely due to thin cloud. Figure 1b shows a thinner *b* plume acquired on August 14 at an altitude near 3 km. This plume corresponds to a rise in  $t_f$  (interrupted by the short time period about local midnight when the sun is too low in the sky to satisfy small-value solar air mass ( $m_0$ ) protocols defined in the processing chain) and low *d* values at the same 3 km altitude. The Bruker FTS retrievals showed elevated values relative to a mean seasonal curve for the July 23/24 event, while no measurements were made during the short smoke event of Aug. 14.

[15] The Figure 1 examples include clear sky “events” that preceded the smoke events; this allows one to appreciate the relatively weak but significant optical signal associated with the latter. During these clear periods, one observes an apparent tendency for moderate and periodic increases in AOD and  $t_f$  which peak around local midnight (AOD and  $t_f$  changes of  $< 0.01$ ). This could be a real diurnal variation or it could be associated with artifactual  $1/m_0$ -type variations induced by calibration coefficient errors [Cachorro et al., 2004] and/or changes in system response after the field instrument is deployed (T. F. Eck, personal communication, 2007). Pre- and post-summer calibration coefficients (T. F. Eck, personal communication, 2007) indicated that the relative calibration coefficient change (at 500 nm) was of the wrong sign (0.6%) to explain the local midnight peaking in the clear-sky diurnal variations of Figure 1. Prior to field deployment, the

Figure 1. Optical measurements for two sample smoke events (delineated by the broken purple lines). The top graphs show AOD,  $t_f$  and  $t_c$  variation (500 nm) while the middle and bottom graphs show the temporally synchronized AHSRL b and d profiles (532 nm). The two clear background “events” listed in Table 1 can be observed prior to these two smoke events. The greyish, data-free zones seen in the Aug. 12 AHSRL data are due to temporary problems with the laser output power setting.

Figure 2. Imagery and back-trajectory support for the event of July 23/24 (event 8 in Table 1). MODIS bands 1, 2, 3, 4, 7 correspond to nominal central wavelengths of 645.0, 856.5, 465.6, 553.6, and 2114.1 nm respectively. The dashed, colour-framed areas delineate equivalent areas in only a very rough fashion.

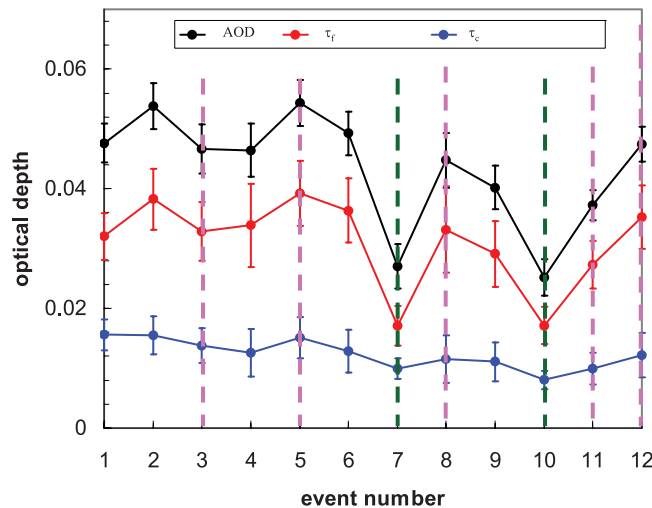


Figure 3. Averaged AOD,  $\tau_f$  and  $\tau_c$  variation for the events of Table 1. The error bars represent calibration errors in the case of the AOD and retrieval errors in the case of  $\tau_f$  and  $\tau_c$ . The pink and green vertical lines represent smoke events and clear-day periods respectively.

calibration coefficient accuracy of AERONET field instruments is generally 1% at 500 nm (T. F. Eck, personal communication, 2007); this error (which could be of either sign), in opposition to the small system degradation error of

0.6% discussed above, would account for only a fraction of the clear-day peaking at local midnight.

[16] An analysis of optical events at the PEARL site was carried out over the summer period of 2007; Figure 3 shows the AOD,  $\tau_f$  and  $\tau_c$  averages as a function of the 12 events defined in Table 1. These events, which were generally fine mode in nature (aside from the “clear” or background periods), were chosen from data acquired during largely cloud-free periods as determined from the b and d profiles and the variation of  $\tau_c$  and  $\tau_f$  (see Table 1 for details). The  $\tau_f$  averages are  $<0.04$ , a value which is near the commonly defined threshold of 0.03 for sub-visual optical events; indeed we had no success in finding visual evidence of smoke in MODIS images acquired over Eureka. The purple broken lines indicate the  $\tau_f$  events which we identified as smoke. The other events were inconclusive as to the source or simply too vertically complex to hope for a simple advective source.

[17] The Table 1 smoke-event sources varied from widely dispersed regions in Russia and Canada. Support for the conclusion that a particular event was due to smoke was (aside from the type of optical behavior seen in Figure 1) provided by back-trajectories, OMI AI (Aerosol Index) data, MODIS imagery of smoke and hotspots, FLAMBE (Fire Locating and Modeling of Burning Emissions) data and Bruker FTS retrievals (when available). In Table 1, Bruker FTS CO and  $C_2H_6$  tropospheric abundances were defined as “enhanced” when at least one measurement during the

Table 1. List of Cloud-Free, Fine-Mode Aerosol Events Identified in AHSRL and PEARL Sunphotometer Data<sup>a</sup>

Event	Period <sup>b</sup>	Comments	Source Date and Source Position <sup>c</sup>	Source Duration <sup>d</sup>
1	May 5–9	No AHSRL data, No enhancement of CO and $C_2H_6$ tropospheric column <sup>e</sup>		
2	May 21–27	Complex AHSRL backscatter structure up to 7–9 km, Tentative CO and $C_2H_6$ enhancement ( $<1s$ )		
3	June 29–30	Single thin-layer smoke plume at 4.5 km. No CO and $C_2H_6$ enhancement	June 25, east of Great Bear Lake, NWT, Canada	June 18 to July 1
4	July 2–3	bi-layer event (4–5 and 9 km). No CO and $C_2H_6$ enhancement		
5	July 10	Enhanced CO and $C_2H_6$ <sup>f</sup>	July 6, south of Great Bear Lake	July 6 to 8
6	July 11	Bi-layer event (2 and 6–7 km). No CO and $C_2H_6$ measurements		
7	July 19–22	Clear background. No CO and $C_2H_6$ enhancement <sup>g</sup>	N/A	N/A
8	July 23/24	Thin-layer plume at 9 km. Enhanced CO and $C_2H_6$	July 18 sources, north of Khabarovsk, Russia	July 14 to July 19
9	July 26–29	Multi-peaked $\tau_f$ event. No CO and $C_2H_6$ enhancement		
10	Aug. 10–13	Clear background. No CO and $C_2H_6$ enhancement	N/A	N/A
11	Aug. 14	Single-layer plume at 3 km. No CO and $C_2H_6$ measurements	Sources north of the Kamchatka Peninsula, Russia <sup>h</sup>	Aug. 3 to Aug. 12
12	Aug. 17–20	Broad-layer smoke dispersed between 0 and 4 km. Enhanced CO and $C_2H_6$ on Aug. 17 and 18 only	Aug. 13, east of Lake Bakail, Siberia	Aug. 11 to Aug. 18

<sup>a</sup>May 1 and August 31, 2007. Cloud-free, fine-mode aerosol events are defined as events for which  $\tau_c < 0.02$  and  $\tau_f > 0.02$ .  $\tau_f$  varies in a systematic temporal fashion (with  $Dt_f > 0.01$ ) and this variation is coherent with b and d variation (as illustrated in Figure 1).

<sup>b</sup>Approximate time duration for which  $\tau_f$  and AHSRL variation indicated a significant fine mode event.

<sup>c</sup>Determined from HYSPLIT back-trajectory analysis applied to the time of a prominent feature in the  $\tau_f$  and AHSRL temporal profiles. Sources, when given without qualification, were supported by the back-trajectories, OMI-AI imagery, FLAMBE emissions and MODIS images of hot spots and/or smoke.

<sup>d</sup>Estimated from OMI-AI data and MODIS colour images. This is more a qualitative indicator of the duration of optically strong smoke near the source (FLAMBE data for example could indicate continued hot-spot activity well outside this time period).

<sup>e</sup>See text for a definition of “enhanced”.

<sup>f</sup>No AHSRL data for most of the day so that the layer height (1–2 km) was derived from plume heights observed at the beginning and end of July 10. No FLAMBE emission data in nominal source region but MODIS imagery shows hot spots and smoke.

<sup>g</sup>Defined as events for which  $\tau_c < 0.02$ ,  $\tau_f < 0.02$  and  $Dt_f < 0.01$ .

<sup>h</sup>The complexity of the meteorology prevented a direct back-trajectory trace to the actual fire sources. For back-trajectory purposes we took the “source” to be the strong smoke plumes seen in MODIS images on Aug. 8 over the East Siberian Sea.

period in question was greater than one standard deviation, corresponding to 6% (CO) or 7% (C<sub>2</sub>H<sub>6</sub>) of the partial column, above the mean temporal curve. We note that due to the limited vertical resolution of the FTS, thin-layer smoke events may not be well captured by this instrument.

[18] It is noteworthy that we could not discern these summertime smoke events from CALIOP profiles acquired from the CALIPSO satellite when it made overflights near Eureka; this is not surprising since the quoted CALIOP minimum detectable  $b$  of  $1.1 \cdot 10^{-3} \text{ km}^{-1} \text{ sr}^{-1}$  [McGill et al., 2007] is near the maximum value of the AHRSL  $b$  values for the weak smoke events which we observed over Eureka ( $\sim 10^{-3} \text{ km}^{-1} \text{ sr}^{-1}$ ; see Figure 1).

[19] The error bars in Figure 3 represent calibration errors for the AOD and derived retrieval errors for  $t_f$  and  $t_c$  [O'Neill et al., 2003]. These error bars assume a nominal AOD error of  $s(\text{AOD}) = \{s(V_0)/V_0\}/m_0$  (where  $m_0$  varied between 2 and 7 during the summer period reported in this paper) and where one assumes a typical AERONET calibration coefficient error of 1% at 500 nm ( $s(V_0)/V_0 = 0.01$ ). As a second, check on retrieval quality, we removed the 1020 nm data from the input AOD spectra to the SDA retrieval. This channel, while it is valuable for its coarse mode information content [O'Neill et al., 2008], suffers from H<sub>2</sub>O vapour absorption and detector temperature sensitivity effects. Although the former problem has been addressed in the AERONET Version 2 processing chain by employing dynamic estimates of H<sub>2</sub>O vapour content from the CIMEL 940 nm channel (B. N. Holben, personal communication, 2006) the current temperature correction is generic (not adapted to each instrument). Retrievals without the 1020 nm channel tended to yield larger values of  $t_f$  than retrievals with this channel. These differences were as large as 0.022 in May and as small as 0.006 in July (corresponding to event-averaged instrumental temperatures of 6.3 and 12.8 C respectively). The spectral reasons for this result were obvious in the data; the 1020 nm AODs were significantly higher than the 870 nm AODs in May (by  $< 100\%$ ; this is physically implausible so that temperature artifacts are highly probable).

## 5. Conclusions

[20] Numerous fine mode (sub-micron) aerosol optical events were observed during the summer of 2007 at the PEARL, high-Arctic atmospheric observatory. Half of these events (the meteorologically simpler, single-layer events) could be traced to forest fires in southern and eastern Russia and the Northwest Territories (NWT) of Canada. The most notable findings were that (a) a combination of ground-based measurements (passive sunphotometry, high spectral resolution lidar) could be employed to determine that weak (near sub-visual) fine mode events had occurred, and (b) this data combined with remote sensing imagery products (MODIS colour and near infra-red imagery, OMI-AI, FLAMBE fire sources), Fourier transform spectrometry and back trajectories could be employed to identify the smoke events.

[21] Acknowledgments. The authors would like to thank three Canadian funding agencies, NSERC, CFCAS, and FQRNT (Québec) for their financial support in the form of individual grants. The authors also gratefully acknowledge NOAA-ARL for access to the HYSPLIT trajectory model, NRL for the use of FLAMBE data and NASA for its MODIS and OMI-AI imagery products available from their Rapidfire, Earth Observatory (natural hazards) and OMI (aerosol) web sites. Logistical and on-site technical support was provided by CANDAC. CANDAC's major Canadian funding sources include CFCAS, NSERC, and CFI. Valuable support was also provided by Environment Canada and NASA's AERONET project. The contributions of Ihab Abboud (Environment Canada), Pierre Fogal, Paul Loewen, Matthew Okraszewski, Alexei Khmel, Oleg Mikhailov, and Ashley Harrett of CANDAC as well as Tom Eck of the AERONET group are gratefully acknowledged. Discussions with Mike Fromm (NRL, Washington) were extremely valuable during the analysis of the smoke events.

## References

- Bodhaine, B. A., and E. G. Dutton (1993), A long-term decrease in Arctic haze at Barrow, Alaska, *Geophys. Res. Lett.*, 20, 947–950.
- Cachorro, V. E., P. M. Romero, C. Toledano, E. Cuevas, and A. M. de Frutos (2004), The fictitious diurnal cycle of aerosol optical depth: A new approach for “in situ” calibration and correction of AOD data series, *Geophys. Res. Lett.*, 31, L12106, doi:10.1029/2004GL019651.
- Eloranta, E. W. (2005), High spectral resolution lidar, in *Lidar: Range-Resolved Optical Remote Sensing of the Atmosphere*, edited by K. Weitkamp, pp. 143–163, Springer, New York.
- Eloranta, E. W., I. A. Razenkov, J. P. Garcia, and J. Hedrick (2006), Observations with the University of Wisconsin Arctic high spectral resolution lidar, paper presented at 22nd International Laser Radar Conference, Int. Coord. Group for Laser Atmos. Stud., Matera, Italy.
- Holben, B. N., et al. (1998), AERONET—A federated instrument network and data archive for aerosol characterization, *Remote Sens. Environ.*, 66(1), 1–16.
- McGill, M. J., M. A. Vaughan, C. R. Trepte, W. D. Hart, D. L. Hlavka, D. M. Winker, and R. Kuehn (2007), Airborne validation of spatial properties measured by CALIPSO lidar, *J. Geophys. Res.*, 112, D20201, doi:10.1029/2007JD008768.
- O'Neill, N. T., T. F. Eck, A. Smirnov, B. N. Holben, and S. Thulasiraman (2003), Spectral discrimination of coarse and fine mode optical depth, *J. Geophys. Res.*, 108(D17), 4559, doi:10.1029/2002JD002975.
- O'Neill, N. T., T. F. Eck, J. S. Reid, A. Smirnov, and O. Pancrati (2008), Coarse mode optical information retrievable using ultraviolet to short-wave infrared Sun photometry: Application to United Arab Emirates Unified Aerosol Experiment data, *J. Geophys. Res.*, 113, D05212, doi:10.1029/2007JD009052.
- Pougatchev, N. S., B. J. Connor, and C. P. Rinsland (1995), Infrared measurements of the ozone vertical distribution above Kitt Peak, *J. Geophys. Res.*, 100(D8), 16,689–16,698.
- Rinsland, C. P., et al. (1998), Northern and southern hemisphere ground-based infrared spectroscopic measurements of tropospheric carbon monoxide and ethane, *J. Geophys. Res.*, 103(D21), 28,197–28,217.
- Rodgers, C. D. (2000), *Inverse Methods for Atmospheric Sounding: Theory and Practice*, Atmos. Oceanic Planet. Phys. Ser., vol. 2, 256 pp., World Sci., Hackensack, N. J.
- Shaw, G. E. (1982), Atmospheric turbidity in the Polar regions, *J. Appl. Meteorol.*, 21, 1080–1088.
- Stohl, A., et al. (2006), Pan-Arctic enhancements of light absorbing aerosol concentrations due to North American boreal forest fires during summer 2004, *J. Geophys. Res.*, 111, D22214, doi:10.1029/2006JD007216.
- Stone, R. S., G. Anderson, E. Andrews, E. Dutton, J. Harris, E. Shettle, and A. Berk (2007), Incursions and radiative impact of Asian dust in northern Alaska, *Geophys. Res. Lett.*, 34, L14815, doi:10.1029/2007GL029878.
- Zhao, Y., et al. (2002), Spectroscopic measurements of tropospheric CO, C<sub>2</sub>H<sub>6</sub>, C<sub>2</sub>H<sub>2</sub>, and HCN in northern Japan, *J. Geophys. Res.*, 107(D18), 4343, doi:10.1029/2001JD000748.
- K. Baibakov, J. Freemantle, N. T. O'Neill, and O. Pancrati, Centre for Research and Applications in Remote Sensing, Université de Sherbrooke, Sherbrooke, QC J1K 2R1, Canada. (norm.oneill@usherbrooke.ca)
- R. L. Batchelor, R. Lindenmaier, and K. Strong, Department of Physics, University of Toronto, Toronto, ON, Canada.
- E. Eloranta, University of Wisconsin, Madison, WI, USA.
- L. J. B. McArthur, Environment Canada, Toronto, ON, Canada.